Supplement of

An Extended Modal Aerosol Dynamics Model (ExMADv1.0) for Simulating Early Nanoparticle Growth

Qihao Lin et al.

Correspondence to: Jiandong Wang (jiandong.wang@nuist.edu.cn)

Section S1. Condensation kernel

Starting from Eq. (9) in Sect. 2.1.3 of the main text, this section presents the detailed derivation of the condensation kernel and the analytical approximation of the modal-average Kelvin effect. The net change in the k-th moment of mode i due to multi-component condensation can first be written in an explicit size-integral form as follows:

$$\left.\frac{\partial M_{k,i}}{\partial t}\right|_{cond} = \sum_c \int_0^\infty \psi_{k,c}(D_p) \cdot \left[C_{gas,c} - C_{sat,c}(T) \cdot \chi_{i,c} \cdot exp\left(\frac{A_c}{D_p}\right)\right] \cdot n_i(D_p) dD_p \quad \text{(S1)}$$

where the subscripts i and c represent mode i and condensing species c, respectively. $\psi_{k,c}(D_p)$ represents the single-particle kinetic transfer function for the k-th moment. Depending on the transport regime, $\psi_{k,i,c}(D_p)$ scales with particle size as D_p^{k-1} in the free molecular regime and D_p^{k-2} in the near-continuum regime, following Appendix A2 of Binkowski and Shankar (1995). $C_{gas,c}$ represents the ambient gas-phase concentration and the equivalent surface equilibrium concentration of species c. $C_{sat,c}(T)$ is the saturation vapor concentration of species c over a flat surface at a specific temperature T. $\chi_{i,c}$ is the mole fraction in the particle phase. The exponential term represents the rigorous size-dependent Kelvin effect. A_c is the species-specific Kelvin parameter independent of particle size.

By linearity of the integral, Eq. (S1) can be decomposed into a growth term and an evaporation term:

$$\left.\frac{\partial M_{k,i}}{\partial t}\right|_{cond} = G_{k,i} - E_{k,i} \quad \text{(S2)}$$

The first term denotes $G_{k,i}$, represents the condensational growth contribution to the k-th moment of aerosol mode i. $C_{gas,c}$ is independent of D_p and can be taken outside of the integral. The integral can be represented by a moment transfer coefficient $\Psi_{k,i,c}$, which serves as the modal-scale kinetic transfer coefficient for species c acting on the k-th moment of mode i. This coefficient provides a compact modal representation of the condensation kinetics across the free-molecular and near-continuum regimes, as suggested in Appendix A2 of Binkowski and Shankar (1995):

$$G_{k,i} = \sum_c C_{gas,c} \int_0^\infty \psi_{k,c}(D_p) \cdot n_i(D_p) dD_p = \sum_c \Psi_{k,i,c} C_{gas,c} \quad \text{(S3)}$$

The second term represents the effective evaporation flux associated with the equilibrium vapor concentration at the particle surface:

$$E_{k,i} = \sum_c \int_0^\infty \psi_{k,c}(D_p) \cdot C_{sat,c}(T) \cdot \chi_{i,c} \cdot exp\left(\frac{A_c}{D_p}\right) \cdot n_i(D_p) dD_p \quad \text{(S4)}$$

To express $E_{k,i}$ in a form analogous to the growth term, we rewrite it using the same moment transfer coefficient $\Psi_{k,i,c}$:

$$E_{k,i} = \sum_c \Psi_{k,i,c} \cdot C_{sat,c}(T) \cdot \chi_{i,c} \cdot \overline{KE_{i,c}} \quad \text{(S5)}$$

where the product of the last three terms is defined as the equivalent surface equilibrium concentration, denoted by $\overline{C_{eq,\iota,c}}$ in Eq.(10) of the main text. $\overline{KE_{i,c}}$ is the kinetic-weighted modal-average Kelvin factor, expressed as:

$$\overline{KE_{i,c}} = \frac{\int_0^\infty \psi_{k,i,c}(D_p) \cdot exp\left(\frac{A_c}{D_p}\right) \cdot n_i(D_p) dD_p}{\int_0^\infty \psi_{k,i,c}(D_p) \cdot n_i(D_p) dD_p} \quad \text{(S6)}$$

Here, $\overline{KE_{i,c}}$ is defined as a kinetic-weighted average of the size-dependent Kelvin factor over the modal size distribution. The single-particle transfer kernel can be written in the unified form $\psi_{k,i,c}(D_p) \propto D_p^m$, where m = k-1 in the free-molecular regime and m = k-2 in the near-continuum regime. Under this notation, the above expression reduces to:

$$\overline{KE_{i,c}} = \frac{\int_0^\infty D_p^m \cdot exp\left(\frac{A_c}{D_p}\right) \cdot n_i(D_p) dD_p}{\int_0^\infty D_p^m \cdot n_i(D_p) dD_p} \tag{S7}$$

Under typical atmospheric conditions, the Kelvin parameter (A_c) is much smaller than the particle diameter of growing nanoparticles $(A_c \approx D_p)$. Thus, the exponential curvature term can be accurately approximated using a first-order Taylor series expansion:

$$exp\left(\frac{A_c}{D_p}\right) \approx 1 + \frac{A_c}{D_p} \tag{S8}$$

Substituting Eq. (S8) into Eq. (S7) yields:

$$\overline{KE_{i,c}} \approx 1 + A_c \frac{M_{m-1,i}}{M_{m,i}} \tag{S9}$$

For a lognormal size distribution, the k-th moment of mode i can be written analytically as $M_{k,i} = N_i D_{gi}^k exp\left[\frac{k^2}{2} ln^2\sigma_{gi}\right]$. Using the analytical expression of lognormal moments, the ratio $\frac{M_{m-1,i}}{M_{m,i}}$ can be further simplified to a function of the geometric mean diameter D_{gi} and geometric standard deviation σ_{gi}. Substituting k=m-1 and k=m into Eq. (S9), the modal-average Kelvin factor can be expressed as:

$$\overline{KE_{i,c}} \approx 1 + \frac{A_c}{D_{gi} \cdot exp[(m-0.5)ln^2\sigma_{gi}]} \tag{S10}$$

This formulation avoids explicit size integration while retaining the leading-order effect of particle curvature on modal condensation.

Section S2. Coagulation kernel

To evaluate the coagulation terms efficiently, we adopt a Gauss-Hermite quadrature treatment for the binary-collision integrals over the lognormal modal size distributions. Gauss-Hermite Quadrature is widely used to compute integrals where the integrand includes the weight function e^{-x^2}. Its fundamental concept is to approximate the integrals by a numerical summation over a finite set of nodes and weights.

$$\int_{-\infty}^{\infty} f(x)e^{-x^2}dx \approx \sum_{l=1}^{N_l} f(x_l)\omega_l \tag{S11}$$

where N_l is the number of quadrature points (nodes). x_l are the nodes, which are the roots of the Hermite polynomial. ω_l are the corresponding weights. $f(x)$ is a user-specified function.

Starting from Eq. (S11), and more generally for all coagulation terms in Eqs. (S19)–(S27), the coagulation contribution can be written as a binary-collision integral over two particle diameters:

$$R_{ij}^{(k)} = \int_0^{\infty}\int_0^{\infty} f\left(D_{p1}, D_{p2}, k\right) n_i(lnD_{p1}) n_j(lnD_{p2}) dlnD_{p1} dlnD_{p2} \tag{S12}$$

where the subscripts i and j refer to particles from two colliding modes. $f\left(D_{p1}, D_{p2}, k\right)$ is the collision integrand for the k-th moment.

For each mode, the particle size distribution is assumed to follow the lognormal form given in Eq. (1) of the main text:

$$n_i\left(\ln D_p\right) = \frac{N_i}{\sqrt{2\pi} ln\sigma_{gi}} \exp[-\frac{(lnD_p - lnD_{gi})^2}{2ln^2\sigma_{gi}}] \tag{S13}$$

To introduce the Gauss-Hermite treatment used in this study, we first consider the one-dimensional quadrature for a single lognormal mode. The integral is transformed into the standard Hermite form by substituting $x = \frac{lnD_p - lnD_{gi}}{\sqrt{2} ln\sigma_{gi}}$:

$$\int_0^{\infty} f(D_p, k) n_i\left(\ln D_p\right) d\ln D_p = \frac{N_i}{\sqrt{\pi}} \int_{-\infty}^{\infty} f(D_p, k) exp(-x^2) dx \approx \frac{N_i}{\sqrt{\pi}} \sum_{l=1}^{N_{node}} f(D_{p,l}, k)\omega_l \tag{S14}$$

$$D_{p,l} = D_{gi} \exp(\sqrt{2} x_l ln\sigma_{gi}) \tag{S15}$$

Because coagulation involves two colliding particles, the above one-dimensional transformation can be extended to two-dimensional Gauss-Hermite quadrature:

$$\int_0^{\infty}\int_0^{\infty} f\left(D_{p1}, D_{p2}, k\right) n_i(lnD_{p1}) n_j(lnD_{p2}) dlnD_{p1} dlnD_{p2} \approx \frac{N_i N_j}{\pi} \sum_{l=1}^{N_{node}} \sum_{q=1}^{N_{node}} f(D_{p,l}, D_{p,q}, k)\omega_l \omega_q \tag{S16}$$

$$D_{p,l} = D_{gi} \exp(\sqrt{2} x_l ln\sigma_{gi}) \tag{S17}$$

$$D_{p,q} = D_{gj} \exp(\sqrt{2} x_q ln\sigma_{gj}) \tag{S18}$$

For intramodal coagulation, both particle diameters are sampled from the same mode, whereas for intermodal coagulation the two diameters are sampled independently from modes i and j, respectively. In this study, we use 10 quadrature points from Abramowitz and Stegun (1965). The abscissas and weights are listed in Table S1.

Table S1. Abscissas and weight for Hermite integration.

$\pm x_l$	ω_l
0.34290	6.10862e-1
1.03661	2.40138e-1
1.75668	3.38744e-2
2.53273	1.34364e-3
3.43616	7.64043e-6

Using the above two-dimensional quadrature framework, the coagulation terms for the nucleation, Aitken, and accumulation modes can be written explicitly. The coagulation terms for the nucleation mode are described by:

$$\frac{\partial M_{k,Nuc}}{\partial t}|_{Nuc-Nuc} = \int_0^\infty \int_0^\infty f_1(D_{p1}, D_{p2}, k) n_{Nuc}(lnD_{p1})\, n_{Nuc}(lnD_{p2}) dlnD_{p1} dlnD_{p2} \quad \text{(S19)}$$

$$\frac{\partial M_{k,Nuc}}{\partial t}|_{Nuc-Ait} = \int_0^\infty \int_0^\infty f_2(D_{p1}, D_{p2}, k) n_{Nuc}(lnD_{p1}) n_{Ait}(lnD_{p2}) dlnD_{p1} dlnD_{p2} \quad \text{(S20)}$$

$$\frac{\partial M_{k,Nuc}}{\partial t}|_{Nuc-Acc} = \int_0^\infty \int_0^\infty f_2(D_{p1}, D_{p2}, k) n_{Nuc}(lnD_{p1}) n_{Acc}(lnD_{p2}) dlnD_{p1} dlnD_{p2} \quad \text{(S21)}$$

The coagulation terms for the Aitken mode are described by:

$$\frac{\partial M_{k,Ait}}{\partial t}|_{Ait-Ait} = \int_0^\infty \int_0^\infty f_1(D_{p1}, D_{p2}, k) n_{Ait}(lnD_{p1}) n_{Ait}(lnD_{p2}) dlnD_{p1} dlnD_{p2} \quad \text{(S22)}$$

$$\frac{\partial M_{k,Ait}}{\partial t}|_{Ait-Nuc} = \int_0^\infty \int_0^\infty f_3(D_{p1}, D_{p2}, k) n_{Nuc}(lnD_{p1}) n_{Ait}(lnD_{p2}) dlnD_{p1} dlnD_{p2} \quad \text{(S23)}$$

$$\frac{\partial M_{k,Ait}}{\partial t}|_{Ait-Acc} = \int_0^\infty \int_0^\infty f_2(D_{p1}, D_{p2}, k) n_{Ait}(lnD_{p1}) n_{Acc}(lnD_{p2}) dlnD_{p1} dlnD_{p2} \quad \text{(S24)}$$

The coagulation terms for the accumulation mode are described by:

$$\frac{\partial M_{k,Acc}}{\partial t}|_{Acc-Acc} = \int_0^\infty \int_0^\infty f_1(D_{p1}, D_{p2}, k) n_{Acc}(lnD_{p1}) n_{Acc}(lnD_{p2}) dlnD_{p1} dlnD_{p2} \quad \text{(S25)}$$

$$\frac{\partial M_{k,Acc}}{\partial t}|_{Acc-Nuc} = \int_0^\infty \int_0^\infty f_3(D_{p1}, D_{p2}, k) n_{Nuc}(lnD_{p1}) n_{Acc}(lnD_{p2}) dlnD_{p1} dlnD_{p2} \quad \text{(S26)}$$

$$\frac{\partial M_{k,Acc}}{\partial t}|_{Acc-Ait} = \int_0^\infty \int_0^\infty f_3(D_{p1}, D_{p2}, k) n_{Ait}(lnD_{p1}) n_{Acc}(lnD_{p2}) dlnD_{p1} dlnD_{p2} \quad \text{(S27)}$$

The function $f_1(D_{p1}, D_{p2}, k)$, $f_2(D_{p1}, D_{p2}, k)$ and $f_3(D_{p1}, D_{p2}, k)$ are defined by:

$$f_1(D_{p1}, D_{p2}, k) = \left[\frac{1}{2}(D_{p1}^3 + D_{p2}^3)^{\frac{k}{3}} - D_{p1}^k\right] \beta(D_{p1}, D_{p2}) \quad \text{(S28)}$$

$$f_2(D_{p1}, D_{p2}, k) = -D_{p1}^k \beta(D_{p1}, D_{p2}) \quad \text{(S29)}$$

$$f_3(D_{p1}, D_{p2}, k) = \left[(D_{p1}^3 + D_{p2}^3)^{\frac{k}{3}} - D_{p2}^k\right] \beta(D_{p1}, D_{p2}) \quad \text{(S30)}$$

Section S3. Gaussian Mixture Model (GMM)

As a generative statistical model, GMM approximates observed aerosol size data with arbitrarily complex shapes to be a combination of multiple unimodal Gaussian distributions (Crawford, 2020; Taylor et al., 2014). This approach has the advantage of effectively decomposing a multimodal aerosol size distribution into interpretable Gaussian-like subpopulations. The equation for multimodal fitting of aerosol size distribution has the form:

$$n_i(\ln D_p) = \sum_{i=1}^{n} a_i \exp[-\frac{(lnD_p - b_i)^2}{c_i^2}] \quad \text{(S31)}$$

where a_i, b_i and c_i are fitting parameters for mode i. Note that in this equation, the size distribution is fitted using a mixture of normal distributions in the lnD_p space rather than lognormal distributions in the D_p domain. The lognormal distribution is skewed in linear space, which can misleadingly appear as inherent asymmetry in the fitted peaks. In contrast, normal distribution is symmetric in lnD_p space. Consequently, the deviation of fitting results will not be attributed to the inherent skewness property of size distribution. This approach allows for a more interpretable decomposition of multimodal size distribution. After a_i, b_i and c_i are obtained at the 95 % level of confidence (p = 0.05), the original lognormal distribution can be constructed based on the relation between fitting parameters (a_i, b_i and c_i) and microphysical parameters (N_i, D_{gi}, and σ_{gi}):

$$N_i = \sqrt{\pi} a_i c_i \quad \text{(S32)}$$

$$D_{gi} = \exp(b_i) \quad \text{(S33)}$$

$$ln\sigma_{gi} = \frac{c_i}{\sqrt{2}} \quad \text{(S34)}$$

Section S4. Model Evaluation

The normalized mean error (NME), the normalized mean bias (NMB) and the root mean square error (RMSE) are used to describe model the model performance in simulating particle size distribution and number concentration:

$$NME = \frac{\sum_{i=1}^{N}|S_i - O_i|}{\sum_{i=1}^{N} O_i} \tag{S35}$$

$$NMB = \frac{\sum_{i=1}^{N}(S_i - O_i)}{\sum_{i=1}^{N} O_i} \tag{S36}$$

$$RMSE = \sqrt{\frac{\sum_{i=1}^{N}(S_i - O_i)^2}{N}} \tag{S37}$$

where S_i and O_i are the simulated and observed variables. N denotes the number of samples during the NPF event.

Figure. S1 to S6

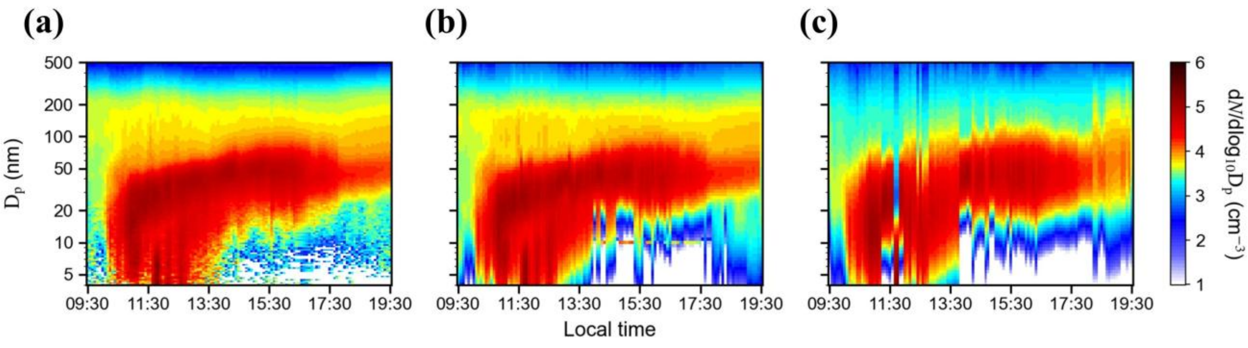

Figure S1. Temporal evolution of PSD during Event 2. (a) The observed PSD. (b) Reconstructed PSD based on the conventional bimodal decomposition. (c) Reconstructed PSD based on the nucleation-resolved three-mode decomposition. The color bar shows the log scale of PSD.

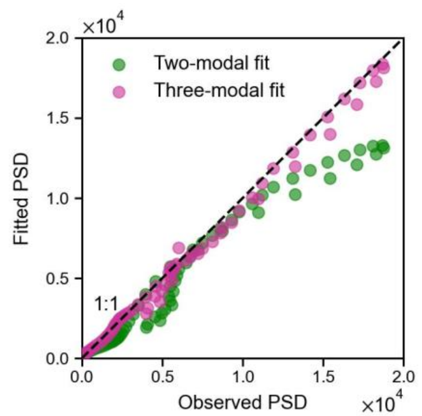

Figure S2. Scatter plot of PSD reconstructed from the two decomposition schemes as a function of the observed PSD for Event 2. The PSDs are time-averaged over the entire NPF period. The bimodal decomposition results are represented by green circles, and the nucleation-resolved decomposition results are shown as magenta circles. The black dashed line indicates the 1:1 reference line.

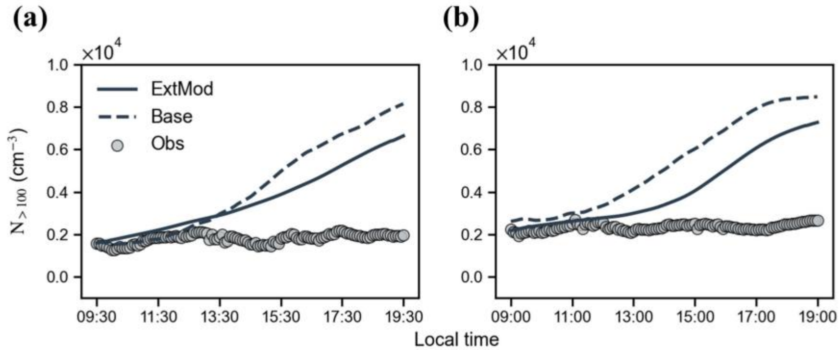

Figure S3. Temporal evolution of particle number concentrations larger than 100 nm ($N_{>100}$) for (a) Event 1 and (b) Event 2. The scatter points represent observational data derived from particle size distributions, while the dashed and solid lines denote the simulation results from the Base scenario and the ExtMod scenario.

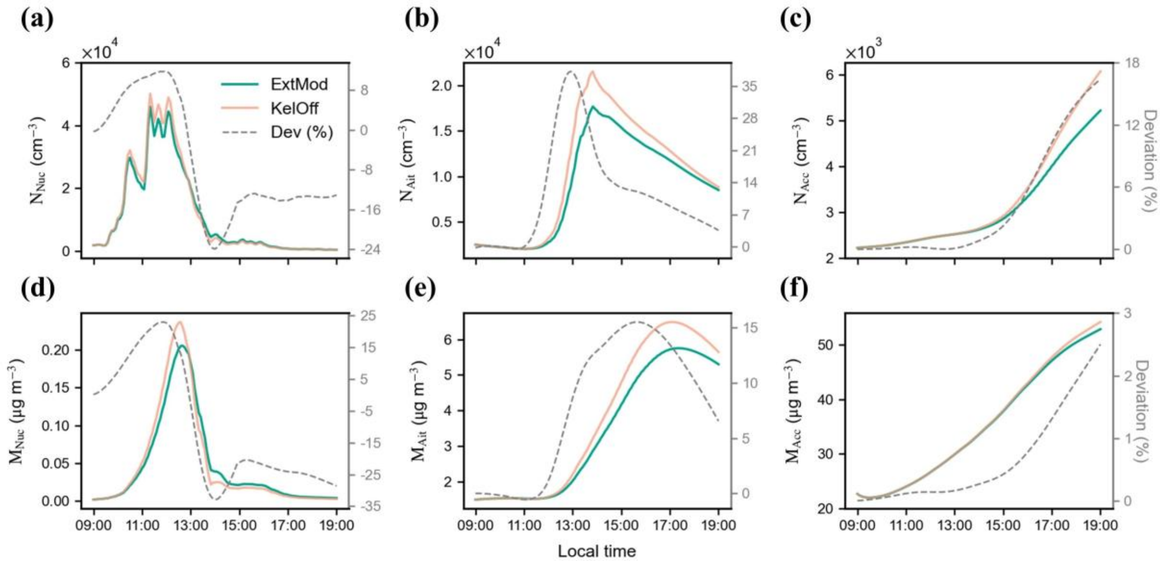

Figure S4. Sensitivity analysis of modal number and mass concentrations to the Kelvin effect for Event 2. Panels (a)–(c) show the temporal evolution of number concentrations in the nucleation, Aitken, and accumulation modes, respectively, and panels (d)–(f) show the corresponding mass concentrations. The green and orange solid lines represent the ExtMod and KelOff simulations, respectively, while the gray dashed lines denote the deviation between KelOff and ExtMod.

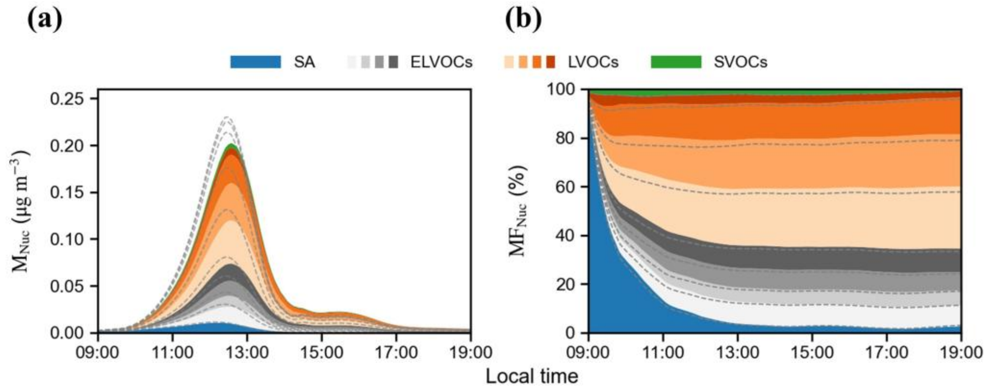

Figure S5. Analysis of the Kelvin effect's impact on the component of particles in the nucleation mode for Event 2. The temporal evolution of (a) mass fraction and (b) mass concentration (unit: μg m^{-3}). The solid line and dashed line denote the ExtMod scenario and KelOff scenario, respectively. The numbers in the legend denote the saturation concentration of OOMs, i.e., C_n^*. OOMs with C_n^* less than 10^{-9} μg m^{-3} are all grouped into category "≤ 10^{-9}". OOMs with C_n^* greater than 10^{-4} μg m^{-3} are uniformly classified as "≥ 10^{-4}".

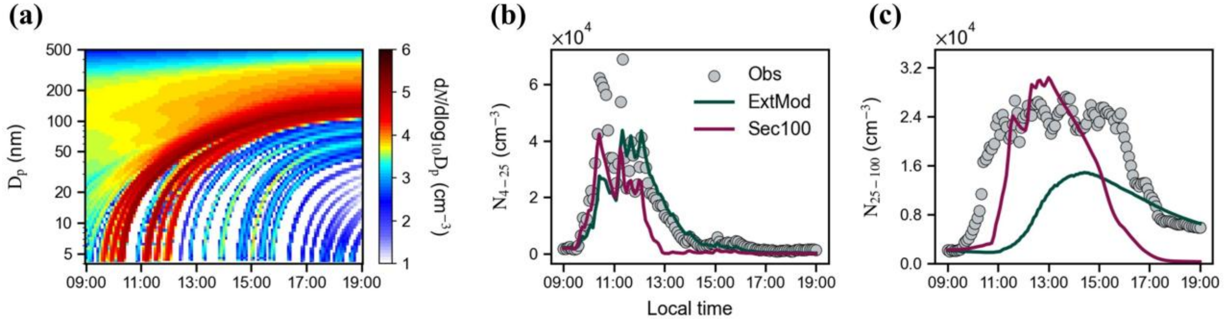

Figure S6. Comparison between the extended modal scheme and the high-resolution sectional scheme for Event 2. Panel (a) shows the particle size distribution (PSD) simulated by the 100-bin sectional configuration (Sec100). Panels (b) and (c) compare the temporal evolution of particle number concentrations in the 4-25 nm (N_{4-25}) and 25-100 nm (N_{25-100}) size ranges, respectively. Grey circles denote observations, and the green and purple lines represent the ExtMod and Sec100 simulations.

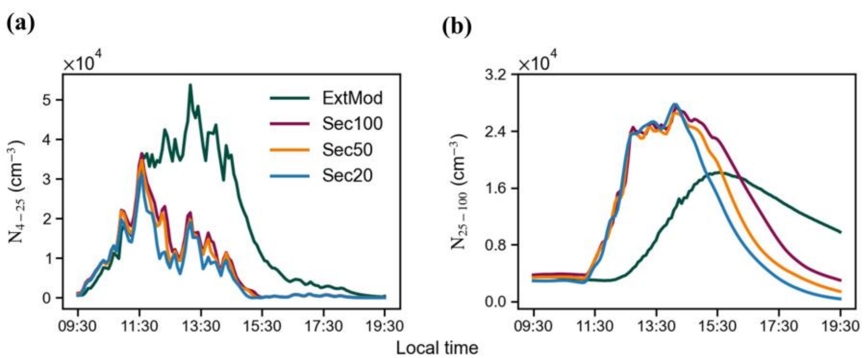

Figure S7. Sensitivity of the sectional-model results to bin resolution for Event 1. Panels (a) and (b) compare the temporal evolution of particle number concentrations in the 4-25 nm (N_{4-25}) and 25-100 nm (N_{25-100}) size ranges, respectively, simulated by the extended modal scheme (ExtMod) and the sectional scheme with 20, 50, and 100 size bins (Sec20, Sec50, and Sec100).

Table. S2 to S7

Table S2. Multimodal fit performance of particle size distribution.

	Event 1			Event 2		
	NME	NMB	RMSE	NME	NMB	RMSE
Two-modal fit	0.10	-0.03	1070.0	0.21	-0.20	1889.7
Three-modal fit	0.04	-0.02	550.4	0.05	-0.04	481.8

Table S3. Metrics of model evaluation in simulating particle number concentration in sub-25 nm size range (N_{4-25}).

	Event 1		Event 2	
	Base	ExtMod	Base	ExtMod
Observation (cm^{-3})	2.18×10^4	2.18×10^4	1.25×10^4	1.25×10^4
Simulation (cm^{-3})	1.01×10^4	1.68×10^4	5.48×10^3	1.06×10^4
NME	0.54	0.27	0.56	0.36
NMB	-0.54	-0.23	-0.56	-0.16
RMSE	1.61×10^4	7.81×10^3	1.22×10^4	8.34×10^3

Table S4. Metrics of model evaluation in simulating particle number concentration in 25-100 nm size range (N_{25-100}).

	Event 1		Event 2	
	Base	ExtMod	Base	ExtMod
Observation (cm^{-3})	1.25×10^4	1.25×10^4	1.65×10^4	1.65×10^4
Simulation (cm^{-3})	1.54×10^4	1.01×10^4	1.10×10^4	8.27×10^3
NME	0.26	0.29	0.41	0.53
NMB	0.23	-0.19	-0.34	-0.50
RMSE	3.58×10^3	5.09×10^3	8.16×10^3	1.11×10^4

Table S5. Metrics of model evaluation in simulating particle number concentration larger than 50 nm ($N_{>50}$).

	Event 1		Event 2	
	Base	ExtMod	Base	ExtMod
Observation (cm^{-3})	5.28×10^{3}	5.28×10^{3}	6.82×10^{3}	6.82×10^{3}
Simulation (cm^{-3})	1.13×10^{4}	8.31×10^{3}	1.09×10^{4}	8.76×10^{3}
NME	1.13	0.66	0.59	0.47
NMB	1.13	0.58	0.59	0.29
RMSE	7.05×10^{3}	4.90×10^{3}	5.20×10^{4}	4.52×10^{3}

Table S6. Metrics of model evaluation in simulating particle number concentration larger than 100 nm ($N_{>100}$).

	Event 1		Event 2	
	Base	ExtMod	Base	ExtMod
Observation (cm^{-3})	1.80×10^{3}	1.80×10^{3}	2.34×10^{3}	2.34×10^{3}
Simulation (cm^{-3})	4.21×10^{3}	3.65×10^{3}	5.29×10^{3}	4.08×10^{3}
NME	1.34	1.02	1.26	0.74
NMB	1.34	1.02	1.26	0.74
RMSE	5.02×10^{3}	2.31×10^{3}	3.60×10^{3}	2.35×10^{3}

Table S7. Metrics of model evaluation in simulating $N_{<25}$ and N_{25-100} for Sec100 scenario.

	Event 1		Event 2	
	$N_{<25}$	N_{25-100}	$N_{<25}$	N_{25-100}
Observation (cm^{-3})	2.18×10^{4}	1.25×10^{4}	1.25×10^{4}	1.65×10^{4}
Simulation (cm^{-3})	7.97×10^{3}	1.33×10^{4}	7.01×10^{3}	1.12×10^{4}
NME	0.64	0.06	0.44	0.40
NMB	-0.63	0.44	-0.44	-0.33
RMSE	1.89×10^{4}	6.25×10^{3}	8.50×10^{3}	8.29×10^{3}

References

Abramowitz, M. and Stegun, I. A.: Handbook of Mathematical Functions: With Formulas, Graphs, and Mathematical Tables, Courier Corporation, 1066 pp., 1965.

Binkowski, F. S. and Shankar, U.: The Regional Particulate Matter Model: 1. Model description and preliminary results, J. Geophys. Res. Atmospheres, 100, 26191–26209, https://doi.org/10.1029/95JD02093, 1995.

Crawford, A.: The Use of Gaussian Mixture Models with Atmospheric Lagrangian Particle Dispersion Models for Density Estimation and Feature Identification, Atmosphere, 11, 1369, https://doi.org/10.3390/atmos11121369, 2020.

Taylor, M., Kazadzis, S., and Gerasopoulos, E.: Multi-modal analysis of aerosol robotic network size distributions for remote sensing applications: dominant aerosol type cases, Atmospheric Meas. Tech., 7, 839–858, https://doi.org/10.5194/amt-7-839-2014, 2014.